# The Effects of Stress, Temperature, and Spin Flips on Polarization Switching in Vertical-Cavity Surface-Emitting Lasers

Guy Van der Sande, Michael Peeters, *Member, IEEE*, Irina Veretennicoff, Jan Danckaert, *Member, IEEE*, Guy Verschaffelt, and Salvador Balle, *Member, IEEE*

***Abstract*—We discuss the effect of uniaxial planar stress on polarization switching in vertical-cavity surface-emitting lasers (VCSELs). The approach is based on an explicit form of a frequency-dependent complex susceptibility of the uniaxially stressed quantum-well semiconductor material. In this mesoscopic framework, we have taken cavity anisotropies, spin carrier dynamics, and thermal shift of the gain curve into account. In this way, we present a model that provides a global overview of the polarization switching phenomenon. The results are compared with experiments on an air-post VCSEL operating at 980 nm.**

***Index Terms*—Numerical analysis, optical polarization, quantum theory, stress, surface emitting lasers.**

## I. Introduction

VERTICAL-CAVITY surface-emitting lasers (VCSELs) are of particular interest because they offer several advantages compared to conventional edge-emitting lasers. They show an improved beam quality, they exhibit low threshold currents and high efficiency, and their parallel growth allows for on wafer testing. One of the most intriguing properties of VCSELs lies in their polarization behavior, which differs from the one of edge-emitting lasers due to the lack of a dominating polarization selection mechanism in the quasi-cylindrically symmetric structure [1]. Usually VCSELs emit linearly polarized light. The polarization direction exhibits a certain randomness, with preferences, however, for the $[1\bar{1}0]$ and [110] crystallographic directions. This has been attributed to an inherent birefringence in the cavity caused by stresses and strain unintentionally induced during manufacturing [2]–[4], and/or to the electrooptic effect arising from the drive voltage [5], [6]. Furthermore, it has been observed that often this linear polarization can switch between two orthogonal states while preserving operation in the fundamental transverse mode of the laser [7]–[10].

Experiments described in [11] show that a mechanical stress, applied externally to the VCSEL package, dramatically alters its polarization behavior. These $P$–$I$ (optical output power versus injected current) measurements on an oxide-confined VCSEL show that the switching current changes when the stress is applied. This work proves the importance of stress on the quantum-well (QW) gain spectra and henceforth on the polarization selection in VCSELs. It is clear from these and other experiments by van Doorn *et al.* [3], [4], Verschaffelt *et al.* [9], Panajotov *et al.* [11], [12], Peeters *et al.* [13], and Sondermann *et al.* [14] that stress plays a crucial role on the polarization properties of VCSELs.

Different physical models have been investigated in the literature to describe polarization switching (PS) in VCSELs. The first model is of thermal nature and attributes PS to a spectral shift of the gain maximum with respect to the cavity resonances for the two frequency-split polarization modes [15]. Extending this idea one can also explain PS due to thermal lensing [16], or by incorporating the temperature and frequency dependence of both losses and gain [17]. A distinctively different model called the spin-flip model (SFM) for PS is developed in [18] and is extended to include frequency and gain anisotropies in [19]. This model describes the active semiconductor QW in terms of a spin-split two-level system, where the two spin subsystems are coupled through spin-flip processes. These two effects, temperature and spin-flip processes, have been combined by Balle *et al.* [20] by introducing an approximate frequency-dependent susceptibility for QW media [21]. This approach permits to include the thermal shift of the cavity resonances over the gain spectrum of the system, and has allowed reproduction of the experimental observations of PS [20], [22] two-frequency emission at threshold [23], and the emission of elliptically polarized states [14]. In all these modeling attempts, strain effects are introduced phenomenologically through the dichroism and birefringence parameters. These parameters, which as already commented describe the residual anisotropies in the structure that may result from unintentional residual strain left after the growth process or from the electrooptic or elastooptic effects in the VCSEL cavity [5], play a key role in the preference for a particular polarization orientation.

Manuscript received March 9, 2006; revised May 10, 2006. This work was supported in part by the European RTN network VISTA under Contract HPRN-CT-2000-00034 and the COST 288 action, and in part by the Interuniversity Attraction Pole program (IAP V/18), in part by the Concerted Research Action "Photonics in Computing", and in part by the Research Council of the Vrije Universiteit Brussel. The work of G. Van der Sande, G. Verschaffelt, and J. Danckaert was supported in part by the Fund for Scientific Research—Flanders (FWO). The work of S. Balle was supported in part by the Ministerio de Ciencia y Tecnología, Spain, through Project TIC2002-04255-C04-03.

G. Van der Sande is with the Department of Applied Physics and Photonics (TW-TONA),Vrije Universiteit Brussel, 1050 Brussels, Belgium and also with the Optique Nonlinéaire Théorique, Université Libre de Bruxelles, 1050 Brussels, Belgium (e-mail: guy.van.der.sande@vub.ac.be).

M. Peeters, I. Veretennicoff, J. Danckaert, and G. Verschaffelt are with the Department of Applied Physics and Photonics (TW-TONA), Vrije Universiteit Brussel, 1050 Brussels, Belgium (e-mail: mpeeters@vub.ac.be; ivereten@vub.ac.be; jandan@vub.ac.be; gverscha@vub.ac.be).

S. Balle is with the Departamento de Física Interdisciplinar, Instituto Mediterráneo de Estudios Avanzados, Consejo Superior de Investigaciones Científicas, Universitat de les Illes Balears, E-07071 Palma de Mallorca, Spain (e-mail: salvador@imedea.uib.es).

Digital Object Identifier 10.1109/JQE.2006.879816

0018-9197/$20.00 © 2006 IEEE

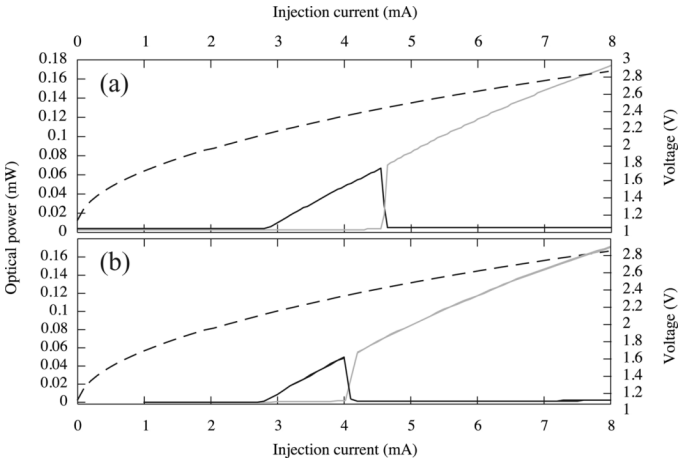


Fig. 1. Typical polarization-resolved PI plots (full lines) and voltage versus current characteristics (dashed line) of the air-post VCSEL. (a) No stress and a frequency splitting of the two linearly polarized modes of −10.8 GHz. (b) With stress and a frequency splitting of −7.5 GHz. The black line corresponds to the high-frequency mode and the gray line corresponds to the low-frequency mode.

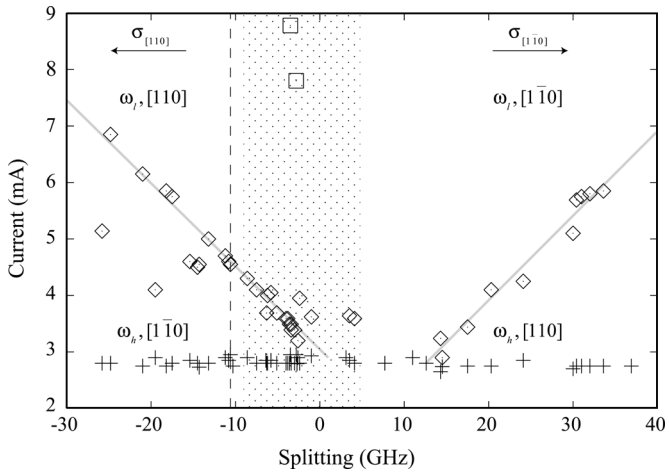


Fig. 2. Value of the switching currents as a function of the frequency splitting between the two linearly polarized modes for the air-post VCSELs. The crosses indicate the threshold current (which is almost constant), the diamonds are the position of the type-I polarization switches and the squares are the type-II switches. At a frequency splitting of −10.8 GHz no stress is applied to the VCSEL structure (indicated by the dashed line). To the left of this line, tensile stress is applied along the [110] direction ($\sigma_{[110]}$), to the right the tensile stress is along [1$\bar{1}$0] ($\sigma_{[1\bar{1}0]}$). In the dotted region, the polarization changes from splitting to splitting. The gray lines are intended to guide the eye.

The goal of this paper is to extend the SFM incorporating a realistic frequency-dependent susceptibility of uniaxially stressed active QW structures recently derived in [24]. This enables us to study the effect of mechanical stresses on the linear stability of the polarization modes. The comparison of these theoretical results with the experiments shows the interplay between the effects of stress in the QW and in the passive sections of the VCSEL cavity. Also, in this way, we have combined the three main origins of PS in VCSELs: temperature effects, spin-flip processes, and stress. As such, we present a rather simple model with still a global picture of the polarization switching phenomenon in VCSELs. The paper is organized in the following way. In Section II, we summarize the relevant experimental results. Section III is dedicated to stress-dependent optical susceptibility function of an active QW. The rate equation model is introduced in Section IV. We study the effect of uniaxial stress on the polarization stability of VCSELs within the framework of SFM (Section V). In Section VI, we compare the theory with the experimental results and show that it is necessary to take into account the elastooptic effect in the passive sections of the device. Section VII contains our conclusions.

## II. Experimental Results

Some of us have shown that mechanical stress, externally applied to the VCSEL package, dramatically alters its polarization behavior [11], [12]. The additional stress will be applied along either the [1$\bar{1}$0] or [110] crystallographic axes by mounting the packaged device into a custom made mechanical holder [25]. The emitted light is collimated. The axes of the birefringence are determined by rotating a polarizer in the beam and looking for the maximum and minimum transmission. Once the main axes are known, the current is scanned, measuring the emitted power along these (linear) polarization directions.

The experimental results have been performed on air-post (index-guided) VCSELs from Avalon Photonics (formerly CSEM) [9], operating around 980 nm. The device has three 8-nm-thick InGaAs QWs embedded in 10-nm-thick GaAs barriers and has GaAs–AlGaAs mirrors. In Fig. 1(a), the polarization resolved optical output power versus injected current curve and the corresponding voltage versus current characteristic are shown for this air-post VCSEL. All measurements have been conducted at a fixed substrate temperature of 25 °C. At this substrate temperature, type-I PS (i.e., from the higher frequency mode to the lower frequency mode) is observed. In this case, when no stress is applied to the VCSEL package, the high-frequency mode ($\nu_h$ state) is selected at threshold and this mode is linearly polarized along the [1$\bar{1}$0] direction. When the injection current is increased a type-I PS around 4.8 mA occurs and the orthogonally polarized low-frequency mode ($\nu_l$ state) becomes stable. Note that a small hysteresis (or bistable region) can be observed around the switching point. The frequency splitting between the two linearly polarized modes is 10.8 GHz. In Fig. 1(b), an example is shown of what occurs when an uniaxial planar stress along [1$\bar{1}$0] is applied to the VCSEL structure. In this case, the switching current moves to 4.0 mA and the frequency splitting between the two polarization modes changes to 7.5 GHz. In the remainder of this paper, we will study these changes in more detail.

Two situations are investigated depending on the orientation of the laser wafer with respect to the direction of the uniaxial stress. In Fig. 2, we have plotted the value of the switching currents (in fact the lower current bound of a small bistable region) as a function of the frequency splitting between the two linearly polarized modes. The frequency splitting is positive when the [110] polarization direction is selected at threshold and negative when the [1$\bar{1}$0] polarization is selected. The crosses in Fig. 2 denote the measured threshold current (which is almost constant), the diamonds indicate the position of the type-I polarization switches and the squares the type-II switches. When no stress is applied to the VCSEL, the splitting equals −10.8 GHz and a type-I PS is observed at 4.8 mA (dashed line in Fig. 2). If uniaxial tensile stress is applied parallel to the [110] direction (to the left from the dashed line in Fig. 2), the switching point will move to higher currents with increasing stress, while the

frequency splitting will increase. The lines in Fig. 2 guide the eye. The spread on the measurement points is largely due to the mechanical relaxation of the VCSEL and its mount.

If uniaxial tensile stress is applied along the $[1\bar{1}0]$ direction (right from the dashed line in Fig. 2), the type-I switching current decreases. In the dotted region, the polarization of the high-frequency mode develops a small ellipticity and its main axis moves towards the [100] direction. This polarization rotation due to stress has been previously studied by some of us in [13]. At frequency splittings around $-3.5$ GHz and an orientation of the linearly polarized mode of 15° off [100], a type-II switch is observed (at currents of around 7.5 mA). When the stress along the $[1\bar{1}0]$ direction is increased, the ellipticity disappears and the orientation of the linearly polarized mode swings towards the [110] direction through a region where no switching is present and the low-frequency mode is always lasing. When the frequency splitting reaches 14.5 GHz a type-I switch reappears while the polarization direction of the high-frequency mode coincides with the [110] direction. Again, with increasing stress, the splitting increases and the switching current moves to higher values. The main goal of this paper is to study this shift in type-I switching current.

Describing the influence of stress theoretically, in order to have a predictive model, is a huge challenge. First, it involves a full microscopical description of the semiconductor medium taking into account stress-induced changes in the band structure of the QW including the band mixing effect between the heavy and light hole states. Second, a model should be developed for the dynamics of the vectorial electric fields in the cavity coupled to the dynamics of electrons and holes in the active region. Third, a full bifurcation analysis of the model needs to be performed to study the polarization stability.

## III. Optical Susceptibility

The optical field is described in terms of the slowly varying amplitudes of its circularly polarized components, $E_\pm$, each interacting with spin channels with electron densities $N_\pm$ [18], [20]. The carrier densities $N_\pm$ tend to be equalized by spin-flip processes. The spin-flip rate of the electrons $\gamma_j$ is much smaller than that of the holes allowing the assumption of equal hole densities. The interaction of a monochromatic circularly polarized wave and the uniaxially stressed active QW is described through a complex susceptibility. The analytical expression presented below results from a calculation of the low temperature susceptibility, assuming that band mixing effects are taking into account up to first order [24]. Taking only the electron and (mixed) heavy hole band into account, it is found that the susceptibility tensor can be split in a contribution of the spin-up channel and the spin-down channel, $\bar{\bar{\chi}} = \bar{\bar{\chi}}_+ + \bar{\bar{\chi}}_-$, with [24]

$$\bar{\bar{\chi}}_+(\omega_+,\omega_-,D_+,D_-) = \begin{pmatrix} 0 & S_+(u_-,D_+,D_-) \\ -S_+(u_+,D_+,D_-) & G_+(u_-,D_+,D_-) \end{pmatrix} \quad (1)$$

$$\bar{\bar{\chi}}_-(\omega_+,\omega_-,D_+,D_-) = \begin{pmatrix} G_-(u_+,D_+,D_-) & S_-(u_-,D_+,D_-) \\ -S_-(u_+,D_+,D_-) & 0 \end{pmatrix} \quad (2)$$

where

$$G_\pm(u,D_+,D_-) = -\frac{\chi_0}{2}\left[\ln\left(1-\frac{2D_\pm}{u+i}\right)+\ln\left(1-\frac{D_++D_-}{u+i}\right)-\ln\left(1-\frac{b}{u+i}\right)\right] \quad (3)$$

$$S_\pm(u,D_+,D_-) = iS_0\frac{\sigma_{[110]}-\sigma_{[1\bar{1}0]}}{u-u_\sigma}\cdot[G_\pm(u,D_+,D_-)-G_\pm(u_\sigma,D_+,D_-)] \quad (4)$$

where $D_\pm = N_\pm/N_t$ is the carrier density per spin channel normalized to the total transparency carrier density. The parameter $b$ sets the background index of refraction and absorption of the unpumped active region. $\chi_0$ is the device-dependent parameter that determines the material gain. $\sigma_{[110]}$ ($\sigma_{[1\bar{1}0]}$) is the strength of the tensile stress applied to the VCSEL structure along the [110] ($[1\bar{1}0]$) direction. $S_0$ is a measure of the stress induced splitting and $u_\sigma$ is a measure of the energy splitting between opposite spin states

$$u_\sigma = -i - u_{\sigma 0} - u_{\sigma 1}\left(\sigma_{[110]}+\sigma_{[1\bar{1}0]}\right). \quad (5)$$

The dependence on the frequency of the field arises through

$$u_\pm = \frac{\omega_\pm}{\gamma_\perp} + \Delta + \rho(D_++D_-)^{1/3} + \delta\left(\sigma_{[110]}+\sigma_{[1\bar{1}0]}\right) \quad (6)$$

where $\Delta = (\Omega-\omega_t)/\gamma_\perp$ is the detuning between the cavity resonance $\Omega$ and the nominal transition frequency $\omega_t$, normalized to the linewidth $\gamma_\perp$, of the optical transition for fixed crystal momentum. The stress induced red-shift is modeled by $\delta$. Bandgap renormalization effects have been taken into account through the phenomenological parameter $\rho$ which describes the bandgap shrinkage with carrier density. All material parameters can be found in Table I with their typical values obtained for an 8-nm $In_{0.2}Ga_{0.8}As$ QW sandwiched between GaAs (see [24]).

## IV. Dynamical Equations

The rate equations of the SFM extended to include the spectral dependence of the material response are [26]

$$\dot{E}_\pm(t) = -\kappa E_\pm + i\frac{a\Gamma}{2}P_\pm \mp (i\gamma_a-\gamma_p)E_\mp, \quad (7)$$

$$\dot{D}_\pm(t) = \frac{\mu}{2} - AD_\pm - BD_\pm^2 - \gamma_j(D_\pm - D_\mp) + \frac{a\varepsilon_0}{2i}\left[(\bar{\bar{\chi}}_\pm\vec{E})\vec{E}^* - c.c.\right] \quad (8)$$

$$\begin{pmatrix} P_+ \\ P_- \end{pmatrix} \approx \varepsilon_0\chi\left(i\frac{\dot{E}_+}{E_+}, i\frac{\dot{E}_-}{E_-}, D_+, D_-\right)\begin{pmatrix} E_+ \\ E_- \end{pmatrix} \quad (9)$$

where $a = \Omega/n_e n_g$ is a linear gain factor with $n_e$ and $n_g$ the effective and group refractive index [26]. $\gamma_p$, the birefringence, and $\gamma_a$, the dichroism, are the anisotropies of the modes linearly polarized along $[1\bar{1}0]$ and [110]. The birefringence $\gamma_p$ can be obtained from a measurement of the frequency splitting.

TABLE I
PARAMETERS

| | | |
|---|---|---|
| $\varepsilon_0 a \chi_0$ | effective gain constant | 4 $10^4$ns$^{-1}$ |
| $\Gamma$ | confinement factor | 0.045 |
| $\gamma_\perp$ | material polarization decay | 10ps$^{-1}$ |
| $\kappa$ | mirror losses | 300ns$^{-1}$ |
| $\gamma_a$ | linear dichroism | 0-1.0ns$^{-1}$ |
| $\gamma_p$ | linear birefringence | 6-30ns$^{-1}$ |
| $A$ | non-radiative recombination rate | 1.0ns$^{-1}$ |
| $B$ | bimolecular recombination rate | 0.1ns$^{-1}$ |
| $\gamma_j$ | spin flip rate | 15ns$^{-1}$ |
| $S_0$ | gain splitting strength | -3.25 $10^{-8}$ m$^2$/N |
| $b$ | total energy spread | 2 $\cdot 10^4$ |
| $u_{\sigma 0}$ | intra band energy gap | -15.42 |
| $u_{\sigma 1}$ | stress-induced intra band energy gap | -2.60 $10^{-8}$ m$^2$/N |
| $\rho$ | band gap renormalization | 0.2 |
| $\delta$ | stress-induced redshift | -7.56 $10^{-9}$m$^2$/N |

For reasons of simplicity, these anisotropies are assumed to be aligned with the external stress directions. $\Gamma$, the confinement factor, and $\kappa$, the photon decay rate, can be calculated from the device structure and the mirror reflectivities. $\mu$ is the renormalized injection current. $A$ and $B$ are the non-radiative and the bimolecular carrier recombination rates for which we have taken the typical values of 1.0 and 0.1 ns$^{-1}$. Spin-flip relaxation processes are modeled by the spin-flip rate, $\gamma_j$. We would like to remark that there exists some debate about the value of the spin-flip rate $\gamma_j$ and that a rather low value is chosen in this paper (15 ns$^{-1}$) to be able to enhance the SFM dynamics. However, the results in Section VI do not depend on this value. The meaning of the different parameters and typical values used here are summarized in Table I. The field is normalized such that the squared field amplitudes are proportional to the photon densities. To simplify the analysis, we assume that the principle axes of the anisotropies and the directions of stress are aligned with the [1$\bar{1}$0] and [110] crystallographic axes. This model will therefore not strictly apply to the dotted region in Fig. 2 where the polarization of the modes develops a slight ellipticity and its main axis changes continuously due to a small residual stress present in the structure. The model can be extended to take into account arbitrary stress and anisotropy axes. However, this will complicate the linear stability analysis of the polarization modes.

The two linearly polarized steady states of (7)–(9) are aligned along the [110] and [1$\bar{1}$0] crystallographic axes. These solutions can be written as

$$E_\pm^{x(y)}(t) = Q_{x(y)} e^{-i\left(\omega_{x(y)} t \mp \psi_{x(y)}\right)} \tag{10}$$

$$D_\pm^{x(y)} = D_{x(y)} \tag{11}$$

with $\psi_x = +\pi/4$ in the [110]-polarized mode and $\psi_y = -\pi/4$ in the [1$\bar{1}$0]-polarized mode. These modes and their linear stability in the case without stress have been studied in [20].

## V. Stress-Dependent Bifurcations

We perform a linear stability analysis of the linearly polarized solutions of (7)–(9). Specifically, the stability of a particular solution is studied by writing it as

$$E_\pm^{x(y)} = \left(Q_{x(y)} + a_\pm\right) e^{-i\left(\omega_{x(y)} t \mp \psi_{xy}\right)} \tag{12}$$

$$D_\pm^{x(y)} = D_{x(y)} + d_\pm \tag{13}$$

where $a_\pm$ is a complex perturbation of the field amplitude and $d_\pm$ is a small perturbation related to the carrier variables. After substituting the perturbed solution given by (12) and (13) in the model (7)–(9) and linearizing the result to first order in the perturbations, one obtains a set of linear coupled differential equations. Due to the alignment of the stress directions and the cavity anisotropies, the stability analysis of the linearly polarized modes is strongly simplified. Just like in the standard SFM, the set of equations can be decoupled into two independent third-order subsets by rewriting the perturbation variables as $S = a_+ + a_-$ and $R = a_+ - a_-$. The first subset describes the stability of the linearly polarized modes to intensity perturbations, while the other describes the polarization stability.

Thermal effects will be modeled by a dependence of the detuning $\Delta$ on temperature. In a full microscopic approach evolution equations for the lattice and electron plasma temperatures should be integrated with the rest of the carrier and field equations. In our mesoscopic approach here, we are only interested in the average temperature of the active QW. From this point of view, we can easily model the relative thermal shift between cavity resonances and the material gain spectrum by a temperature dependent detuning. As the gain spectrum red shifts about four to five times faster than the cavity frequencies, increasing temperature will correspond to increasing $\Delta$. We consider that the thermal shift of the cavity resonance over the gain spectrum is the dominant mechanism for thermal roll-over, and we disregard changes in the material gain and transparency carrier densities.

Keeping in mind that the detuning represents temperature, we construct bifurcation diagrams in the $(\Delta, \mu)$-plane from the linear stability analysis of the linearly polarized solutions. In a first step, we will study how the stress dependent susceptibility tensor influences the possible switching scenarios predicted by the SFM. We have plotted the bifurcation diagrams in Figs. 3 and 4 for a tensile stress applied in the [110] and the [1$\bar{1}$0] direction, respectively. In these figures, we have deliberately taken a rather low value of the spin-flip rate (15 ns$^{-1}$) and appropriate values for the birefringence (15 ns$^{-1}$) and the dichroism (1 ns$^{-1}$), such that the dynamic effects due to spin flips become very apparent. In Fig. 3, tensile stress is applied in the [110]-direction only and so the mode polarized along [1$\bar{1}$0] becomes more stable when the stress is increased. This is of course related to the gain splitting due to stress. The opposite case is depicted in Fig. 4. The bifurcation diagram without stress is the

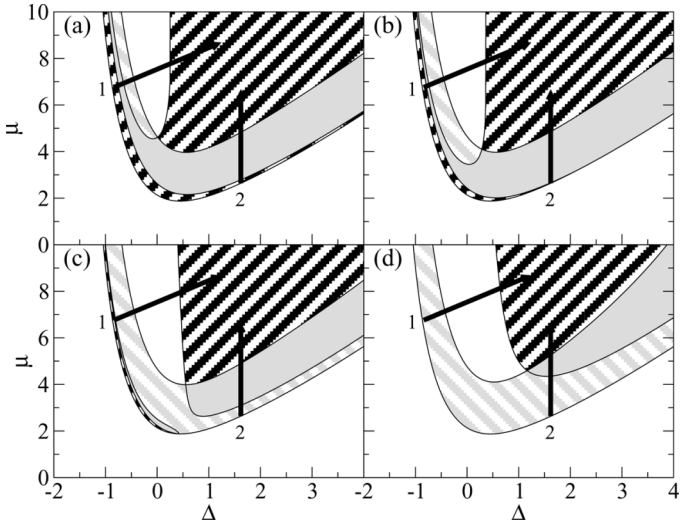


Fig. 3. Current-detuning linear stability diagram for the linearly polarized solutions. The lower curves give the dependence of the threshold current on the detuning $\Delta$. The parameters used are presented in Table I and $\gamma_j = 15\ \mathrm{ns}^{-1}$, $\gamma_p = 15\ \mathrm{ns}^{-1}$, $\gamma_a = 1\ \mathrm{ns}^{-1}$, $\sigma_{[1\bar{1}0]} = 0$ Pa and (a) $\sigma_{[110]} = 0$ Pa, (b) $\sigma_{[110]} = 10^5$ Pa, (c) $\sigma_{[110]} = 2 \cdot 10^5$ Pa, and (d) $\sigma_{[110]} = 5 \cdot 10^5$ Pa. The fill indicates the polarization direction: ///:[110] and \ \ \ : $[1\bar{1}0]$. The gray hatching strokes indicate that the low-frequency mode is stable, while the black hatching strokes denote a stable high-frequency mode. A full gray region indicates bistability. A white region above threshold indicates that no linearly polarized mode is stable.

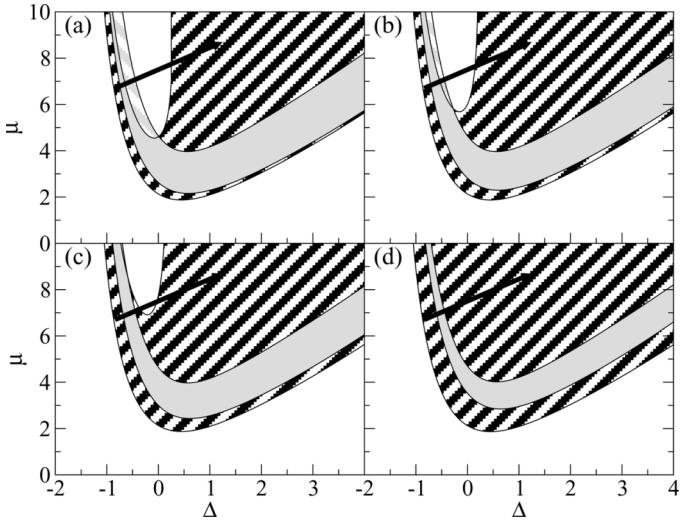


Fig. 4. Current-detuning linear stability diagram for the linearly polarized solutions. The lower curves give the dependence of the threshold current on the detuning $\Delta$. The parameters used are presented in Table I and $\gamma_j = 15\ \mathrm{ns}^{-1}$, $\gamma_p = 15\ \mathrm{ns}^{-1}$, $\gamma_a = 1\ \mathrm{ns}^{-1}$, $\sigma_{[1\bar{1}0]} = 0$ Pa and (a) $\sigma_{[1\bar{1}0]} = 0$ Pa, (b) $\sigma_{[1\bar{1}0]} = 10^5$ Pa, (c) $\sigma_{[1\bar{1}0]} = 2 \cdot 10^5$ Pa, (d) $\sigma_{[1\bar{1}0]} = 5 \cdot 10^5$ Pa. The definitions of the fills can be found in the caption of Fig. 3.

same as in Fig. 3(a), but now stress is applied in the orthogonal direction. Clearly, now the [110]-polarized mode is preferred with increasing stress [Figs. 4(b)–(d)]. To discuss the effect of the stress on possible switching scenarios, we consider two trajectories (indicated by the arrows numbered 1 and 2) in the $(\Delta, \mu)$-space. Paths Nr. 1 and 2 were chosen such that typical SFM switches can be studied. Path Nr. 1 is a prototypical path when thermal drift of the cavity resonance is important. Path Nr. 2 has a constant detuning and so does not take thermal heating into account. However, it has its significance when the VCSEL is driven with a pulsed current with low duty cycle short pulses in order not to heat the device. In this case only changes due to carrier dynamics will occur, which have been taken into account by the susceptibility.

In the absence of stress [see Fig. 3(a)], path Nr. 1 describes a consecutive type-I and type-II switch. At threshold, the high-frequency mode is selected. It switches through a bistable region to the low-frequency mode (type-I switch). At a higher current, the low-frequency mode loses stability and a switch occurs to the high-frequency mode through a region of stable elliptically polarized modes and dynamical states. These situations have been previously found in this region in other works [14], [27], [28]. When the stress is increased [see Fig. 3(b)–(d)], the type-I switch occurs at a lower current. When it hits threshold, the low-frequency mode will be selected at threshold. The lower bifurcation current of the region of instabilities corresponding with the type-II switch is unaffected, while the upper boundary moves to higher currents with increasing stress.

If we follow path Nr. 2 in Fig. 3(a), the high frequency mode is selected at threshold. At higher currents, the low-frequency mode is also stable, but for even higher currents again only the high-frequency mode remains stable. When the stress is increased [see Fig. 3(c)], the low-frequency mode will be selected at threshold and a type-II switch will occur to the high-frequency mode. For even larger stress [see Fig. 3(d)], the switching moves to a higher current. For higher values of the spin-flip rate, the dynamical regions move to higher currents. However, the stabilization due to stress of one of the polarization modes occurs in a similar way as discussed above.

The switching scenario in Fig. 4(a) is the same as the one followed by arrow Nr. 1 in Fig. 3(a). If tensile stress is applied along the $[1\bar{1}0]$ crystallographic axes, the region where the low-frequency mode is stable and the region of instabilities move to higher currents. As a result, the type-I PS has completely disappeared in Fig. 4(c), although a passage through the region of instabilities persists. For more stress, in Fig. 4(d), no switching occurs.

The frequency splitting between the two linearly polarized modes remains more or less fixed throughout the switching scenarios presented in this Section. This is due to the fact that the stress-dependent susceptibility only models the elastooptic effect within the QW, while surely the elastooptic effect acts in all the passive sections of the VCSEL structure. A proper inclusion of this effect is necessary to compare with experimental results. Therefore, we will consider the elastooptic effect in the next Section.

## VI. Comparison With the Experiments

To compare with the experiments, we have performed the previous analysis with a value for the birefringence which approximately corresponds to the measured frequency splitting of 10.8 GHz $(-30\ \mathrm{ns}^{-1})$. We neglect the dichroism $\gamma_a = 0\ \mathrm{ns}^{-1}$. The results can be found in Fig. 5 for stress applied to $[1\bar{1}0]$ direction and Fig. 6 for [110]. In the unstressed case, in Figs. 5(a) and 6(a), the high-frequency mode ($[1\bar{1}0]$ polarized) is selected at threshold at the low frequency side of the gain curve, while

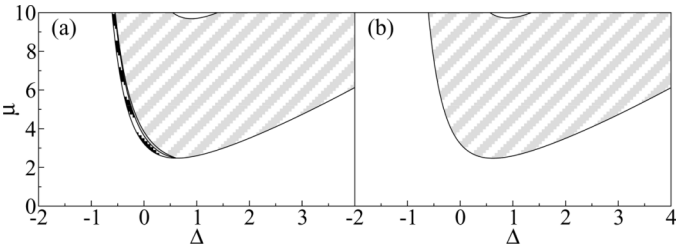


Fig. 5. Current-detuning linear stability diagram for the linearly polarized solutions account. The lower curves give the dependence of the threshold current on the detuning $\Delta$. The parameters used are presented in Table I and $\gamma_j = 15\ \mathrm{ns}^{-1}$, $\gamma_p = -30\ \mathrm{ns}^{-1}$, $\gamma_a = 0\ \mathrm{ns}^{-1}$, $\sigma_{[110]} = 0$ Pa and (a) $\sigma_{[1\bar{1}0]} = 0$ Pa, (b) $\sigma_{[1\bar{1}0]} = 3 \cdot 10^5$ Pa. The definitions of the fills can be found in the caption of Fig. 3.

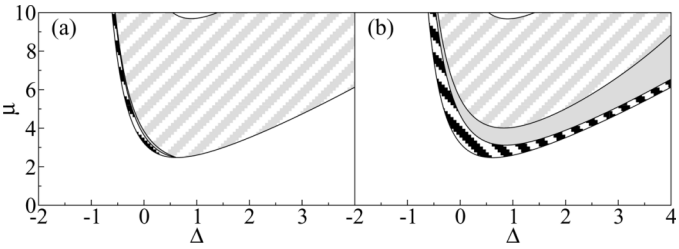


Fig. 6. Current-detuning linear stability diagram for the linearly polarized solutions account. The lower curves give the dependence of the threshold current on the detuning $\Delta$. The parameters used are presented in Table I and $\gamma_j = 15\ \mathrm{ns}^{-1}$, $\gamma_p = -30\ \mathrm{ns}^{-1}$, $\gamma_a = 0\ \mathrm{ns}^{-1}$, $\sigma_{[1\bar{1}0]} = 0$ Pa and (a) $\sigma_{[110]} = 0$ Pa, (b) $\sigma_{[110]} = 3 \cdot 10^5$ Pa. The definitions of the fills can be found in the caption of Fig. 3.

at the high frequency side the low-frequency mode ([110] polarized) is selected. A small region of bistability exists and at higher currents a region of instabilities or possible elliptically polarized states emerges. When stress is applied along $[1\bar{1}0]$ in Fig. 5(b), the low-frequency mode polarized along [110] will be stabilized for all detunings, while when stress is applied along [110] in Fig. 6(b), the high-frequency mode becomes more stabilized at threshold and the bistable region becomes broader and moves to higher currents. Clearly, Fig. 5(b) does not correspond to the experimental results as for large stress values no switching can occur and only the low-frequency mode will lase. Also, for all stress values, the frequency splitting between the two linearly polarized modes remains more or less unchanged. To be able to reproduce the experimental results, we need to take into account the elastooptic effect.

In a cylindrical VCSEL, apart from the effects of stress considered in the previous Sections there exists an in-plane anisotropy for the refractive index due to electro- and elastooptically induced birefringence. The electrooptical contribution is mainly due to the applied voltage and the built-in voltages at the many heterojunctions in the distributed Bragg reflectors [5]. The elastooptical contribution arises from residual strain on top of which we add external stress [13]. Assuming that the axes of the residual birefringence $\gamma_{p0}$ are aligned with the [110] and $[1\bar{1}0]$ directions, we model the elastooptic effect as

$$\gamma_p = \gamma_{p0} - \gamma_{p\sigma}\left(\sigma_{[110]} - \sigma_{[1\bar{1}0]}\right) \tag{14}$$

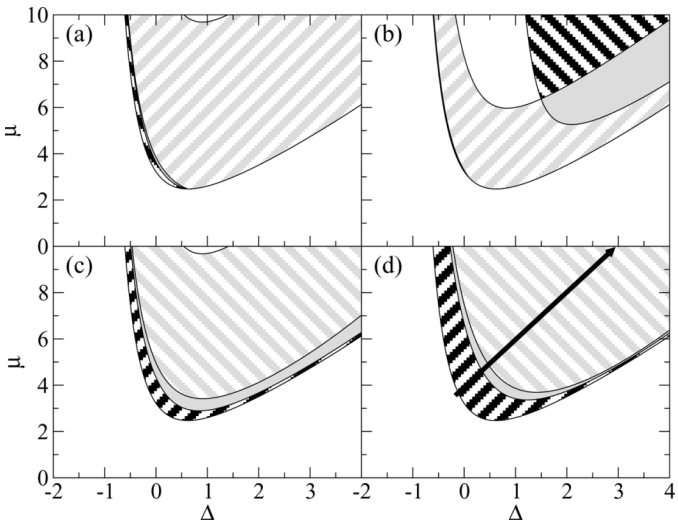


Fig. 7. Current-detuning linear stability diagram for the linearly polarized solutions taking the elastooptic effect into account. The lower curves give the dependence of the threshold current on the detuning $\Delta$. The parameters used are presented in Table I and $\gamma_j = 15\ \mathrm{ns}^{-1}$, $\gamma_{p0} = -30\ \mathrm{ns}^{-1}$, $\gamma_{p\sigma} = 3 \cdot 10^{-4}\ \mathrm{ns}^{-1}\mathrm{Pa}^{-1}$, $\gamma_a = 0\ \mathrm{ns}^{-1}$, $\sigma_{[110]} = 0$ Pa and (a) $\sigma_{[1\bar{1}0]} = 0$ Pa, (b) $\sigma_{[1\bar{1}0]} = 5 \cdot 10^4$ Pa, (c) $\sigma_{[1\bar{1}0]} = 2 \cdot 10^5$ Pa, (d) $\sigma_{[1\bar{1}0]} = 3 \cdot 10^5$ Pa. The definitions of the fills can be found in the caption of Fig. 3.

where the frequency of the mode polarized orthogonally to the stress direction is increased with increasing stress strength, while the frequency of the mode polarized along the stress direction is lowered. In principle, through the elastooptic effect also the cavity losses of the two polarizations along the major crystal axes become different. This effect is not taken into account. However, due to the elastooptic effect the frequencies of the polarization modes vary. As such, the modal gains will also change due to the different modal position on the gain curve, which is taken into account by the dispersion in the susceptibility function. We have repeated the linear stability analysis taking (14) into account. The result can be found in Figs. 7 and 8.

For ease of comparison, we have repeated the unstressed case in Figs. 7(a) and 8(a). When the stress is increased in the $[1\bar{1}0]$ direction [see Fig. 7(b)], the splitting decreases and the gain of the [110]-mode will be higher. As a result the region of stable high-frequency mode polarized along $[1\bar{1}0]$ is pushed away. For rather small splittings Fig. 7(b), the region of instabilities has become bigger and a new region of stable high-frequency mode emerges. When the stress is increased the splitting reverses sign and the mode polarized along [110] is now the high-frequency mode Figs. 7(c) and (d). In Fig. 7(c), the high-frequency mode is now selected at threshold for any detuning, followed by a region of bistability. At higher currents the low-frequency mode polarized along $[1\bar{1}0]$ is stable. When the tensile stress is increased further Fig. 7(d), the mode polarized along [110] becomes stable in a larger parameter domain. Following the current-detuning path represented by the arrow in Fig. 7(d), a polarization switch occurs from the high-frequency mode to the low-frequency mode (type-I) and the switching current increases when more stress is applied to the VCSEL structure. This is the same behavior as observed in the experiments.

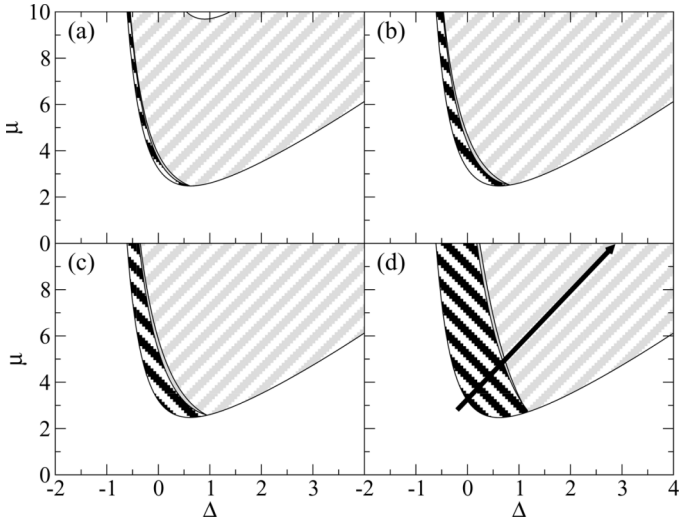


Fig. 8. Current-detuning linear stability diagram for the linearly polarized solutions taking the elastooptic effect into account. The lower curves give the dependence of the threshold current on the detuning $\Delta$. The parameters used are presented in Table I and $\gamma_j = 15\text{ns}^{-1}$, $\gamma_{p0} = -30$ ns$^{-1}$, $\gamma_{p\sigma} = 3 \cdot 10^{-4}$ ns$^{-1}$ Pa$^{-1}$, $\gamma_a = 0$ ns$^{-1}$, $\sigma_{[1\bar{1}0]} = 0$ Pa and (a) $\sigma_{[110]} = 0$ Pa, (b) $\sigma_{[110]} = 5 \cdot 10^4$ Pa, (c) $\sigma_{[110]} = 10^5$ Pa, and (d) $\sigma_{[110]} = 3 \cdot 10^5$ Pa. The definitions of the fills can be found in the caption of Fig. 3.

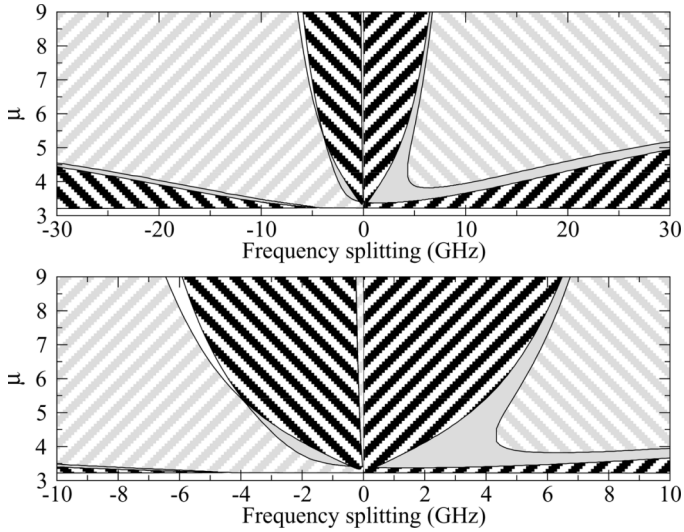


Fig. 9. Current-splitting linear stability diagram for the linearly polarized solutions (the lower panel is an expanded view of the central region in the top panel). The followed current-detuning path starts from $(\Delta = 0, \mu = \mu_{th})$ to $(\Delta = 3, \mu = 10)$. The parameters used are presented in Table I and $\gamma_{p0} = -30$ ns$^{-1}$, $\gamma_{p\sigma} = 3 \cdot 10^{-4}$ ns$^{-1}$Pa$^{-1}$, $\gamma_j = 15$ ns$^{-1}$ and $\gamma_a = 0$ ns$^{-1}$. The definitions of the fills can be found in the caption of Fig. 3.

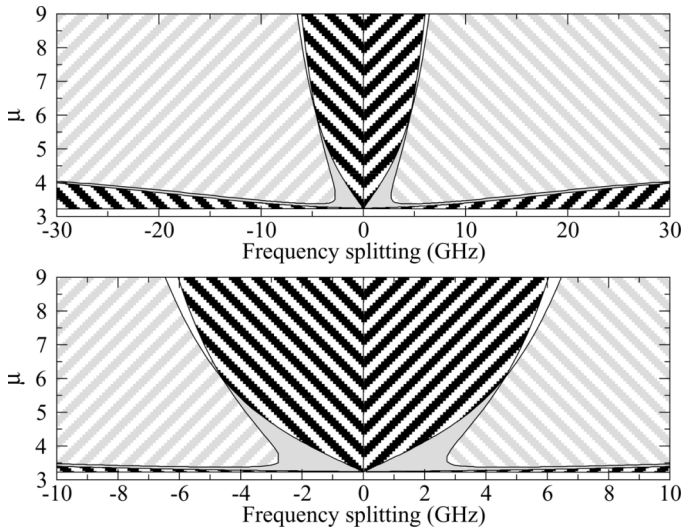


Fig. 10. Current-splitting linear stability diagram for the linearly polarized solutions (the lower panel is an expanded view of the central region in the top panel). The followed current-detuning path starts from $(\Delta = 0, \mu = \mu_{th})$ to $(\Delta = 3, \mu = 10)$. The parameters used are presented in Table I and $\gamma_{p0} = -30$ ns$^{-1}$, $\gamma_{p\sigma} = 3 \cdot 10^{-4}$ ns$^{-1}$Pa$^{-1}$, $\gamma_j = 15$ ns$^{-1}$, $\gamma_a = 0$ ns$^{-1}$ and $S_0 = 0$. The definitions of the fills can be found in the caption of Fig. 3.

For completeness, we have also included the stability diagrams in the case that stress is applied along the [110] direction (Fig. 8). The frequency splitting increases with stress. The $[1\bar{1}0]$-mode becomes even more high frequency, while the other will have a lower frequency with stress. The $[1\bar{1}0]$-mode will also be gain-favored due to the stress-induced gain split. Following the current-detuning path represented by the arrow in Fig. 8(d), a polarization switch occurs from the high-frequency mode to the low-frequency mode (type-I) and the switching current increases when more stress is applied to the VCSEL structure. Again, we observe the same behavior as in the experiments.

Following the current-detuning path as depicted in Figs. 7(d) and 8(d) for different amounts of stress has allowed us to compare theory with experiment. In Fig. 9, we study the stability of the linearly polarized modes varying the current and stress by plotting the bifurcation currents versus the frequency splitting at threshold. The situation without any externally applied stress corresponds to a frequency splitting of $-9.6$ GHz. At this splitting, the high-frequency mode linearly polarized along $[1\bar{1}0]$ is selected at threshold. As the current is increased the system passes through a bistable region and then selects the low-frequency mode linearly polarized along [110]. When stress is applied in the [110] direction, the frequency splitting becomes more negative and the type-I switching region moves to higher currents. If stress is applied in the $[1\bar{1}0]$ direction, the frequency splitting becomes smaller, crosses zero and then grows steadily. The type-I switching current becomes smaller and reaches threshold. At that point the low-frequency mode is selected at threshold, while at higher currents the stability switches to the high-frequency mode (type-II switch). When the frequency splitting crosses zero, the mode polarized along [110] becomes the high-frequency mode and at higher frequency splittings a type-I scenario reappears. The type-I switching current increases with the strength of the tensile stress and with the frequency splitting. Note the clear asymmetry between the negative and positive side of the frequency splitting. If we compare the theoretical Fig. 9 with the experimental Fig. 2, we find a good correspondence. The type-I switching current does indeed increase with increasing tensile stress (or increasing frequency splitting) and around the zero frequency splitting type-II switches appear. One could wonder if the elastooptic effect alone can be responsible for the increase in type-I switching. Therefore, we have redone this study neglecting the effects of stress in the QW [$S_0 = 0$ in (4)]. These results are shown in Fig. 10. Again the type-I and type-II switches can be identified, but this time around the type-I switching current

increases less strongly. Also, the stability picture is completely symmetric for both signs of the frequency splitting. From this we can conclude, that the effects of stress on the QW gain are necessary to correctly describe the influence of tensile stress on the polarization stability of VCSELs. We have repeated the above studies for higher values of the spin-flip rate and have found qualitatively the same results.

## VII. Summary

We have studied the effect of uniaxially planar stress on the current driven polarization switching phenomenon in VCSELs. We have included an analytical susceptibility function, taking effects of uniaxial stress into account, into a rate equation model based on the SFM. Through a linear stability analysis, we have studied the polarization stability of the linearly polarized steady states. We have considered both stress applied to the QW as well as the effect of stress on the entire VCSEL structure. In both cases, the polarization stability is considerably influenced by the stress-induced gain splitting. In the case that the elastooptic effect is taken into account in the entire VCSEL structure, we have shown that for high amounts of stress, the bifurcation scenario reduces to a type-I scheme (from high-frequency mode to low-frequency mode), with a switching current that increases with increasing stress. Type-II switching can be observed only for stresses such that the frequency splitting of the linearly-polarized solutions at threshold is small. This result is in agreement with the experimental results. In this way, we have unified the three main ingredients for polarization switching in VCSELs: thermal effects, spin-flip relaxation processes, and uniaxial stress.

## Acknowledgment

The authors would like to thank T. Erneux for fruitful discussions and the reviewers for their in-depth and stimulating questions.

## References

[1] L. A. Coldren and S. W. Corzine, *Diode Lasers and Photonic Integrated Circuits*. New York: Wiley, 1995.

[2] M. Travagnin, "Linear anisotropies and polarization properties of vertical-cavity surface-emitting semiconductor lasers," *Phys. Rev. A*, vol. 56, pp. 4094–4105, 1997.

[3] A. K. J. van Doorn, M. P. van Exter, and J. P. Woerdman, "Elasto-optic anisotropy and polarization orientation of vertical-cavity surface-emitting semiconductor lasers," *Appl. Phys. Lett.*, vol. 69, pp. 1041–1043, 1996.

[4] ——, "Strain-induced birefringence in vertical-cavity semiconductor lasers," *IEEE J. Quantum Electron*, vol. 34, no. 4, pp. 700–706, Apr. 1998.

[5] M. P. van Exter, A. K. J. van Doorn, and J. P. Woerdman, "Electro-optic effect and birefringence in semiconductor vertical-cavity lasers," *Phys. Rev. A*, vol. 56, pp. 845–853, 1997.

[6] R. F. M. Hendriks, M. P. van Exter, J. P. Woerdman, A. van Geelen, L. Weegels, K. H. Gulden, and M. Moser, "Electro-optic birefringence in semiconductor vertical-cavity lasers," *Appl. Phys. Lett.*, vol. 71, pp. 2599–2601, 1997.

[7] J. Martin-Regalado, J. L. A. Chilla, J. J. Rocca, and P. Brusenbach, "Polarization switching in vertical-cavity surface emitting lasers observed at constant active region temperature," *Appl. Phys. Lett.*, vol. 70, pp. 3350–3352, 1997.

[8] M. San Miguel, *Semiconductor Quantum Optoelectronics*. Bristol, U.K.: Institute of Physics, 1999.

[9] G. Verschaffelt, K. Panajotov, J. Albert, B. Nagler, M. Peeters, J. Danckaert, I. Veretennicoff, and H. Thienpont, "Polarisation switching in vertical-cavity surface-emitting lasers: from experimental observations to applications," *Opto-Electron. Rev.*, vol. 9, no. 3, pp. 257–268, 2001.

[10] T. Ackemann and M. Sondermann, "Characteristics of polarization switching from the low to the high-frequency mode in vertical-cavity surface-emitting lasers," *Appl. Phys. Lett.*, vol. 78, pp. 3574–3576, 2001.

[11] K. Panajotov, B. Nagler, G. Verschaffelt, A. Georgievski, H. Thienpont, J. Danckaert, and I. Veretennicoff, "Impact of in-plane anisotropic strain on the polarization behavior of vertical-cavity surface-emitting lasers," *Appl. Phys. Lett.*, vol. 77, pp. 1590–1592, 2000.

[12] K. Panajotov, B. Nagler, G. Verschaffelt, J. Albert, J. Danckaert, I. Veretennicoff, H. Thienpont, J. Yong, and J. Rorison, "In-plane strain modification of polarization behavior of vertical-cavity surface-emitting lasers," *Proc. SPIE*, vol. 4286, pp. 55–62, 2001.

[13] M. Peeters, K. Panajotov, G. Verschaffelt, B. Nagler, J. Albert, H. Thienpont, I. Veretennicoff, and J. Danckaert, "Polarization behavior of vertical-cavity surface-emitting lasers under the influence of in-plane anisotropic strain," *Proc. SPIE*, vol. 4649, pp. 281–291, 2002.

[14] M. Sondermann, T. Ackemann, S. Balle, J. Mulet, and K. Panajotov, "Experimental and theoretical investigations on elliptically polarized dynamical transition states in the polarization switching of vertical-cavity surface-emitting lasers," *Opt. Commun.*, vol. 235, pp. 421–434, 2004.

[15] K. D. Choquette, D. A. Richie, and R. E. Leibenguth, "Temperature dependence of gain-guided vertical-cavity surface-emitting laser polarization," *Appl. Phys. Lett.*, vol. 64, pp. 2062–2064, 1994.

[16] K. Panajotov, B. Ryvkin, J. Danckaert, M. Peeters, H. Thienpont, and I. Veretennicoff, "Polarization switching in VCSELs due to thermal lensing," *IEEE Photon. Technol. Lett.*, vol. 10, no. 1, pp. 6–8, Jan. 1998.

[17] B. Ryvkin, K. Panajotov, A. Georgievski, J. Danckaert, M. Peeters, G. Verschaffelt, H. Thienpont, and I. Veretennicoff, "Effect of photon-energy-dependent loss and gain mechanisms on polarization switching in vertical-cavity surface-emitting lasers," *J. Opt. Soc. Amer. B, Opt. Phys.*, vol. 16, pp. 2106–2113, 1999.

[18] M. San Miguel, Q. Feng, and J. V. Moloney, "Light-polarization dynamics in surface-emitting semiconductor-lasers," *Phys. Rev. A*, vol. 52, pp. 1728–1739, 1995.

[19] J. Martin-Regalado, F. Prati, M. San Miguel, and N. B. Abraham, "Polarization properties of vertical-cavity surface-emitting lasers," *IEEE J. Quantum Electron.*, vol. 33, no. 5, pp. 765–783, May 1997.

[20] S. Balle, E. Tolkachova, M. San Miguel, J. R. Tredicce, J. Martin-Regalado, and A. Gahl, "Mechanisms of polarization switching in single-transverse-mode vertical-cavity surface-emitting lasers: Thermal shift and nonlinear semiconductor dynamics," *Opt. Lett.*, vol. 24, pp. 1121–1123, 1999.

[21] S. Balle, "Simple analytical approximations for the gain and refractive index spectra in quantum-well lasers," *Phys. Rev. A*, vol. 57, pp. 1304–1312, 1998.

[22] M. Sondermann, M. Weinkath, and T. Ackemann, "Polarization switching to the gain disfavored mode in vertical-cavity surface-emitting lasers," *IEEE J. Quantum Electron.*, vol. 40, no. 1, pp. 97–104, Jan. 2004.

[23] M. Sondermann, M. Weinkath, T. Ackemann, J. Mulet, and S. Balle, "Two-frequency emission and polarization dynamics at lasing threshold in vertical-cavity surface-emitting lasers," *Phys. Rev. A*, vol. 68, no. 3, p. 033822, 2003.

[24] G. Van der Sande, J. Danckaert, I. Veretennicoff, K. Panajotov, and S. Balle, "Analytical approximation for the quantum well gain and refractive index spectra of vertical-cavity surface-emitting lasers including the effect of uniaxial planar stress," *Phys. Rev. A*, vol. 71, no. 6, p. 063801, 2005.

[25] K. Panajotov, H. Thienpont, and I. Veretennicoff, U.S. Patent Application #60/318.530.

[26] J. Mulet, "Semiconductor laser dynamics: Compound-cavity, polarization and transverse modes," Ph.D. dissertation, Univ. Illes Balears, Palma de Mallorca, Spain, 2003.

[27] T. Erneux, J. Danckaert, K. Panajotov, and I. Veretennicoff, "Two-variable reduction of the San Miguel-feng-moloney model for vertical-cavity surface-emitting lasers," *Phys. Rev. A*, vol. 59, pp. 4660–4667, 1999.

[28] F. Prati, P. Caccia, M. Bache, and F. Castelli, "Analysis of elliptically polarized states in vertical-cavity-surface-emitting lasers," *Phys. Rev. A*, vol. 69, no. 3, p. 033810, 2004.

**Guy Van der Sande** was born in Mechelen, Belgium, in 1978, He graduated from the Vrije Universiteit Brussels (VUB), Brussels, Belgium, in 2001 as an Electrical Engineer with majors in applied physics and photonics. In 2005, he received the Ph.D. degree from the Department of Applied Physics and Photonics, VUB, on the subjects of vertical-cavity surface-emitting lasers and nonlinear photonic crystals.

His research interests are in the field of nonlinear semiconductor laser dynamics and in the field of metamaterials for optical applications.

**Michael Peeters** (M'96) was born in Antwerp, Belgium, in 1971 and graduated as an Electronical Engineer with majors in applied physics and photonics in 1995 and received the Ph.D. degree on the subject of polarization switching in vertical-cavity surface-emitting lasers in 2005, both from the Vrije Universiteit Brussel (VUB), Brussels, Belgium.

With this work, he contributed in particular to the development of numerical modeling tools for the analysis of stochastic effects in these lasers. His current activities focus on the spatial coherence properties of semiconductor lasers.

Dr. Peerers is member of the International Society for Optical Engineering.

**Irina Veretennicoff** was born in Antwerp, Belgium, in 1944. She received the Ph.D. degree in physics from the the Vrije Universiteit Brussel (VUB), Brussels, Belgium, in 1973 with a dissertation on the statistical transport theory of relativistic plasmas.

She contributed to the development of the successful Applied Physics Curriculum in the School of Applied Sciences (VUB, 1984), of the Photonics Curriculum for the electrical engineering students (VUB, 1994) and recently to the establishment of the Inter-University Master in Engineering Science: Photonics, with the University of Ghent. Since 1987, she has focused her research efforts on photonics (nonlinear optics, VCSELs, laser dynamics). She has been responsible at the VUB for several Belgian Inter-University Attraction Poles.

Dr. Veretennicoff received the Russian State Prize for Physics and Mathematics in 1990 (with V.V. Belyi and Y.V. KLimontovich) for her research in plasma physics.

**Jan Danckaert** (M'04) was born in Antwerp, Belgium, in 1964. He graduated from the University of Antwerp in physics in 1985. He then joined the Department of Applied Physics and Photonics (TONA), Vrije Universiteit Brussel (VUB), Brussels. Belgium, where he received the Ph.D. degree on the subject of nonlinear optics in 1992.

After a stay abroad in Grenoble, France (1993), he returned to TONA, VUB as a Postdoctoral Research Fellow of the Flemish Fund for Scientific Research (FWO). In 2001 and 2002, he was a Visiting Scientist at Departamento de Física Interdisciplinar, Instituto Mediterráneo de Estudios Avanzados, Consejo Superior de Investigaciones Científicas, Universitat de les Illes Balears (IMEDEA, UIB), Palma de Mallorca, Spain. Since 2005, he has been a Full Professor at the VUB, teaching introductory physics for both science and engineering students. His research interests focus on semiconductor laser dynamics in general and the polarization and noise properties of vertical-cavity surface-emitting lasers (VCSELs) in particular.

**Guy Verschaffelt** was born in Belgium in 1973. He graduated from the Vrije Universiteit Brussels (VUB), Brussels, Belgium, in 1996 as an Electrical Engineer with majors applied physics and photonics. In 2000, he received the Ph.D. from the Department of Applied Physics and Photonics, VUB, on the subject of vertical-cavity surface-emitting lasers for parallel optical interconnections.

Presently, he is working at the Department of Applied Physics and Photonics, VUB, as a Postdoctoral Research Fellow of the Fund for Scientific Research (FWO, Belgium).

**Salvador Balle** (M'91) was born in Manacor, Mallorca, Spain in 1961. He received the Ph.D. degree in physics from the Universitat Autònoma de Barcelona, Barcelona, Spain in 1988.

He is currently with the Institut Mediterrani d'Estudis Avançats, IMEDEA (CSIC-UIB), Campus Universitat de les Illes Balears, Palma de Mallorca, Spain. His research interests are the nonlinear dynamics of semiconductor lasers and amplifiers and the modeling of the nonlinear optical properties of these devices.